On the origin of Umtanum Ridge: kinematics of Neogene slip

Brendan A. Miller

A thesis

submitted in partial fulfillment of the

requirements for the degree of

Master of Science

University of Washington

2014

Committee:

Juliet G. Crider

Darrel S. Cowan

Program Authorized to Offer Degree:

Earth and Space Science

University of Washington

Abstract

On the origin of Umtanum Ridge: kinematics of Neogene slip

Brendan Allen Callaghan Miller

Chair of the Supervisory Committee:
Dr. Juliet G. Crider
Earth and Space Science

Constraining the geometry of active faults is an important step in determining accurate estimates of regional seismic hazard. Where subsurface data are lacking, the shape of hanging wall folds can be used to interpret fault geometry at depth. In order to better understand the seismic hazard posed by the Yakima folds in central Washington, I produced a new geologic map and employ kinematic modeling techniques to probe the geometry of a reverse/thrust fault controlling folding of the Columbia River Basalt flows at Umtanum Ridge near Ellensburg, WA. Depending on the technique used, Umtanum Ridge may have formed from either thin or thick-skinned deformation. My preferred model, using a combination of fault-bend and trishear fault-propagation folding, is consistent will measured flow top attitudes along a line of section through the ridge. This model implies that up to 520 m of slip has occurred since 15.6 Ma on a fault soling in a detachment ~ 4 km deep. The rate of deformation derived from the model underestimates (by a factor of 2) previously published rates derived from both geodetic and geomorphic data, implying that current rates of deformation may be higher than the long term average.

Acknowledgements

I would first like to thank my advisor, Juliet Crider, for guiding me through my graduate school journey with great patience and insight. Though we experimented with a couple different ideas for theses, I knew that whatever topic I landed on I would have Juliet's support. I would also like to thank Darrel Cowan for his advice and extensive knowledge of structural geology, which he is always eager to share.

The genesis of this project owes much to Tom Pratt, who always encouraged me to think big with regard to my work. Harvey Kelsey has been a great resource for bouncing ideas off of, and getting feedback from. Gabe Casale deserves special thanks for introducing me to kinematic modeling software, teaching me the ropes, and numerous conversations about the structures of central Washington. Brian Sherrod provided much of the lidar data that form the basis for all of this work. Other lidar data were readily available to me courtesy of the Puget Sound Lidar Consortium and the NSF EarthScope program via opentopography.org. Special thanks to Jack Powell for making available the archive of unpublished geologic mapping from the field area. My field work was assisted greatly by John Lasher and Ken Eaton. Funding for this project was provided by the Geological Society of America, the USGS NEHRP program, and the Department of Earth and Space Sciences at the University of Washington.

Lastly, I would like to thank my family for always believing in me and encouraging me to explore the world. Their support has been unending and unconditional.

Table of contents

Introduction

Accurate assessments of the seismic hazard posed by active tectonic settings require assumptions regarding the geometry of the faulting. In particular the depth of faulting and, hence, the potential area over which the fault slips, plays a first-order role in determining the magnitude of maximum credible earthquake. In tectonic settings dominated by shortening, the depth of the décollement controls the depth of faulting. In convergent settings where subsurface data are lacking, the geometry of hanging wall folds provides the best way to interpret fault geometries at depth. The goal of this paper is to constrain the geometry of a potentially active thrust fault using kinematic modeling to reproduce the observed hanging wall fold.

The Yakima fold and thrust belt (YFTB) in south-central Washington State consists of several NW-SE to W-E trending anticlinal ridges separated by broad (~20 km) synclinal basins (Figure 1). Generally with steeper northern flanks bounded by thrust or reverse fault traces, the anticlines are thought to represent fault related hanging-wall folds (Bentley, 1977; Goff, 1981; Hagood, 1986; Reidel, 1984, 1989). Within the folds are lava flows of the Miocene (17-6 Ma) Columbia River Basalt Group (CRBG) which were emplaced as quasi-horizontal sheet flows and subsequently folded by underlying thrust or reverse faults (Reidel et al., 1984, 1989). There is evidence that the ridges were uplifting contemporaneously with CRBG emplacement from observations documenting the thinning and on-lapping of CRBG members over and on the ridges (Reidel, 1984). Several lines of evidence suggest that deformation is ongoing and that the faults may pose a seismic hazard. Late-quaternary colluvial deposits are observed to be offset by the Saddle Mountains fault (West et al., 1996) and on the southern flank of Umtanum ridge (Blakely et al., 2011). Geodetic data, recorded by GPS, show active shortening across the Cascadian

backarc region (McCaffery et al., 2000, 2007, 2013; Mazzotti et al., 2002). Inversion of the data across an assumed YFTB crustal bock by McCaffery et al. (2013) yields a permanent shortening rate of 1.9 ± 0.5 mm/yr across the backarc from central Oregon to north-central Washington. It is likely that this convergence rate is partitioned onto multiple faults within the YFTB. Focal mechanisms generally indicate thrust faulting with a significant fraction of events showing strike-slip mechanisms (McCaffrey et al., 2007); however the area's background seismicity does not correlate well with mapped structures (Gomberg et al., 2012).

The Yakima folds lie in an area that is particularly sensitive to seismic hazards. Several major dams, providing electricity and irrigation for the region, impound the Columbia and Snake Rivers at several locations throughout eastern and central Washington. Also located on the Columbia River and within the YFTB region, the Hanford Nuclear Reservation hosts both a functioning nuclear power plant and a nuclear waste storage facility. These critical pieces of infrastructure, as well as several population centers (e.g. Ellensburg, Yakima, Tri-Cities), could be at greater risk from destructive earthquakes than has previously been assumed. Current predicted maximum earthquake magnitudes range from M_w5.2 to M_w7.7 based on probabilistic seismic hazard analyses (Geomatrix Consultants, 1996; Benjamin and Associates et al., 2012). These estimates depend on empirical relationships, including fault geometry, which have never been conclusively determined. The large range in maximum earthquake magnitudes stems from the uncertainty in fault geometry, namely the maximum depth of faulting.

Most previously published studies have interpreted the Yakima folds as an example of "thin-skinned" deformation, where faulting is contained within the basalt. Faults are shown cutting up-section from a relatively shallow detachment located either at the base of the CRBG or in a deeper sedimentary horizon (Bruhn, 1981; Campbell & Bentley, 1981; Watters, 1988; Reidel et

al., 1989). Such an interpretation, if correct, would imply a relatively small seismogenic surface area, assuming the décollement is aseismic, and lower seismic hazard. Alternatively, if the faults extend through the both the CRBG and sedimentary rocks into crystalline basement, then a greater seismic hazard can be inferred, because the faults are larger. This case has been previously hypothesized (Bentley, 1977) and is supported by recent geophysical evidence: gravity data require kilometer scale relief on the interface between Cenozoic sedimentary rocks and the underlying crystalline basement (Saltus, 1993; Blakely et al., 2011). By studying the deformation recorded in the CRBG, I test the competing hypotheses of thin-skinned (shallow décollement) faulting versus deeper, basement involved faulting.

Study area

The study area is centered on the intersection of Umtanum Ridge and the Yakima Canyon, roughly equidistant from the cities of Ellensburg and Selah, Washington (Figure 1). This setting presents the opportunity to examine the geometry of a typical YFTB ridge where it has been incised by a major river, providing excellent exposure. Umtanum Ridge is the topographic expression of the NW-SE trending Umtanum anticline, which folds the Miocene Columbia River Basalt Group (CRBG) and is bounded by a thrust fault on the north side . East of the Yakima River, the ridge is bounded by a second thrust fault on the south side (see Plate 1). On either side of the ridge, synclinal troughs separate Umtanum from the adjacent ridges, Manastash to the north and Umtanum South to the south. The basalt flows exposed in the ridges document deformation from at least 15.6 Ma to present from the emplacement of the Grande Ronde Basalt Formation, the oldest CRBG rocks exposed. It is likely that deformation initiated before this date based on the thinning of basalt flows in the anticlines comprising other Yakima ridges (Reidel, 1984). Beneath the basalt, at an elevation approximately 1 km below sea level, lie continental

sedimentary and volcaniclastic rocks estimated to date from the Eocene and Oligocene, based on the interpretation of a borehole drilled along the axis of the Umtanum Ridge South anticline (Campbell, 1989). The base of the borehole lies at an elevation 4.5 km below sea level in these sedimentary rocks. Another borehole located on the NNW-SSE trending Naneum Ridge-Hog Ranch anticline 40 km NE of the study area penetrates into granitic rocks which may be responsible for long-wavelength gravity anomalies underlying the CRBG in eastern Washington (Blakely et al., 2011). The rocks underlying the CRBG seem speculatively consistent with rocks found in the Cascade Range to the NW, namely the graben-fill sediments of the Eocene Swauk formation underlain by terranes accreted in the Mesozoic such as the Mount Stuart Batholith and Ingalls Complex (Campbell, 1989; Cheney and Hayman, 2009).

Methods

Kinematic modeling forms the basis for determining the origin of Umtanum Ridge. Because fault geometry has a systematic influence on geometric relationships in overlying folded stratigraphy (e.g. Suppe, 1985; Rowen and Linares, 2000; Allmendinger and Shaw, 2000; Wilkerson et al., 2002), estimates of fold geometry based on structural and geologic data can be used to evaluate kinematic models of fault-related folding.

Geologic map

A new geologic map (Plate 1) based on a compilation of sources serves as the data used to constrain kinematic models for the formation of Umtanum ridge. Prior mapping in the area, both published (Bentley and Campbell 1983; Bentley et al. 1993) and unpublished (Jack Powell, written comm.), was compiled and augmented with new original field mapping and image interpretation. Digital elevation models at 1 m per pixel resolution were produced from recently

acquired airborne laser swath mapping (ALSM or LiDAR) (EarthScope; Puget Sound Lidar Consortium, 2010; Army Yakima Training Center provided by Brian Sherrod, written comm.). The DEMs along with field checks helps to confirm locations of contacts in the prior mapping.

Bedding attitudes are an important input into kinematic models of fault-related folding. Flow-top attitudes in the study area were compiled and extracted from prior mapping. Additional attitude data were measured from the high-resolution DEM. This is accomplished by identifying three points on a single surface and defining the strike and dip via a "three-point-problem" in GIS. These and the previously measured attitudes form the basis for the estimation of the geometry of Umtanum Ridge used in conjunction with kinematic modeling.

Following the lead of published mapping at 1:100,000 scale (Schuster, 1994), individual lava flows are grouped into flow-unit members, consisting of geologically contemporaneous flows separated by sediments deposited during volcanic hiatuses. The map units break down as follows:

Quaternary undifferentiated (Qu): Includes modern alluvium and alluvial fans found in and adjacent to the Yakima River and its tributaries. Note that this does not include numerous Quaternary landslides which were not mapped for this study.

Upper flows of Columbia River Basalt Group (CRBu): Includes the Pomona Member of the Saddle Mountains Basalt, Priest Rapids and Roza Members, both of the Wanapum Basalt, as well as the intercalated sedimentary rocks of the Ellensburg Formation. I grouped these members to aid in the structural analysis because they are very thin (10s of meters each) compared to lower units. All these members are older than 12 Ma (Reidel et al. 1989b).

Frenchman Springs Member, Wanapum Basalt (FS): Includes at least two flows in this area, the youngest of which is dated to 15.3 Ma (Reidel et al. 1989b). The underlying Vantage Sandstone of the Ellensburg Formation is also included. The Frenchman springs Member has a maximum thickness of 100 m in the map area.

Upper flows of normal polarity, Grande Ronde Basalt (GRn2): Youngest flows date to 15.6 Ma (Reidel et al. 1989b). This unit has a minimum thickness of 300 m based on the YM 1-33 borehole located adjacent to the Yakima River in the core of the southern anticline in the map area.

Upper flows of reversed polarity, Grande Ronde Basalt (GRr2): Comprised of the uppermost reversely magnetized Grande Ronde Basalt flows. Unit has a minimum thickness of 750 m based on the YM 1-33 borehole (Campbell, 1989).

In comparison with prior work on the nearby Saddle Mountains anticline (Casale, 2012), seismic reflection data at Umtanum ridge are unavailable. One-dimensional subsurface data is available where Shell Oil Company explored Umtanum South anticline with a deep borehole located in Yakima Canyon (Yakima Minerals 1-33; Campbell, 1989; Reidel et al, 1989b). In addition to determining the local thicknesses of Grande Ronde Basalt members and locating the base of the basalt at 1050 m below mean sea level (Reidel et al., 1989b), the well penetrated the terrestrial sedimentary and volcanic rocks underlying the basalt to 4500 m below mean sea level. Campbell (1989) interpreted these rocks to be from (in increasing age) the Ohanapecosh, Roslyn, Teanaway, and Swauk Formations. The well's dip log indicates that these rocks within these formations are likely folded, dipping up to 45° generally towards the SW.

Beyond the well data, geophysical surveys provide some information about the subsurface. Regional gravity data show broad positive anomalies underlying YFTB structures, including Umtanum Ridge, and their associated magnetic lineaments (Blakely et al., 2011). These gravity highs could either represent uplifted pre-Cenozoic crystalline rocks, possibly indicating thick skinned tectonics, or paelotopography on the crystalline basement surface. See the **Discussion** section for further information on the relevance of geophysical data to Umtanum Ridge.

In order to evaluate two-dimensional kinematic models for the formation of Umtanum anticline, I choose the line of section shown on Plate 1 (see "Line of section" in legend). The section spans the anticline from the syncline to the south to the syncline to the north. I chose to locate the section line west of Yakima Canyon because of the structural simplicity of having a single fault to the north in comparison to the east side of the canyon, where the ridge is bounded by two faults on both the north and south. A simple explanation for both faults would have them merging at a relatively shallow depth with one fault representing a back-thrust off of a master reverse or thrust fault. Abundant dip data are located adjacent to the line of section and provide structural control for the kinematic modeling.

Kinematically viable cross sections showing fold-fault relationships can be generated using several different approaches. Two of these methods, fault-propagation folding and fault-bend folding, ensure kinematic viability in that they conserve cross sectional area (in two dimensions) as well as stratigraphic thickness. The third, trishear fault-propagation folding, conserves area but does cause changes in stratigraphic thickness. With these approaches, described hereafter, I will test thick vs. thin skinned faulting.

Fault-propagation folding

Fault propagation folds (FPF) form during the process of fault lengthening, the folding taking place just in front of the propagating fault surface (Figure 2; Suppe, 1985). FPF are observed in contractional settings where major thrusts die out in the cores of folds. They are notable for producing asymmetric folds with steep-to-overturned limbs adjacent to a thrust fault (Suppe and Medwedeff, 1990). The situation at Umtanum Ridge is similar, with steep and overturned dips adjacent to the thrust fault on the north side of the ridge. The FPF model has been used extensively to evaluate fold and fault geometry in thrust settings (e.g. Mitral, 1990; Calabro et al., 2003; Abascal, 2005).

FPFs grow self-similarly through kink-band migration, meaning that the fold maintains the same shape and position relative to the fault tip. The kinked limbs of a FPF are ideally homoclinal, their dips not varying within each of up to three domains. As seen in Figure 2, three dip domains comprise the fold ahead of the propagating fault tip (unfaulted case). Down dip from the fault tip only two dip domains comprise the fold (faulted case). Fault-propagation folds exhibit a geometric relationship between the hinge to limb angles γ and γ^* of the hanging-wall anticline for both unfaulted and faulted cases, respectively, and the fault cutoff angle θ (Figure 2).

I grouped the dip data located within 1 km of the line of section through Umtanum ridge on the west side of the Yakima River into dip domains, two domains to evaluate the possibility of a faulted fault propagation fold, and three domains to evaluate the unfaulted case (Figure 3). I assigned dip data into groups based on their locations projected onto the line of section and where the dips change significantly enough to suggest possible dip domain boundaries. In the faulted case, this requires two populations: a population of steep dips in the forelimb and a more moderately dipping backlimb. Three populations were chosen for the unfaulted case: a forelimb, mid-limb, and backlimb. For each population I calculated the Fisher distribution mean vector

along with the 95% confidence cone (Fisher et al., 1987) of the poles to the planes represented by the dip data. The plane perpendicular to the mean vector defines the mean orientation of each dip domain. I used the mean limb orientations to determine γ and γ^* for the unfaulted and faulted cases, respectively and calculated θ using the equations (Figure 2) of Suppe (1985). Then, using the 95% confidence cone, I alter the limb dips in order to maximize and minimize the values of γ and γ^* and to compute maximum and minimum fault cutoff angles, θ, in each case (Table 1).

Using a combination of Suppe's (1985) method and constraints from the mapped geology, I construct kinematically viable cross sections of Umtanum anticline as a FPF. The hinge-to-limb angles constrain the dip of the fault surface (fault cutoff angle). Further constraints come from the positions of the intersections of geologic contacts and the line of section and the position of the mapped thrust. In the faulted case the position of the mapped thrust constrains the position of the fault at the ground surface. In the unfaulted case the mapped position of the fault represents a dip domain boundary between the steep forelimb dips and the shallow dipping flows to the north. The final fault tip location is along this domain boundary, the axial surface of the FPF syncline. These limit the range of positions of the fault cutoff and the amount of slip, which I determined iteratively using Midland Valley Explorations' *Move* structural modeling and visualization software. In this process, a model of the basaltic section, with initial thickness based on the Yakima Minerals 1-33 borehole and surface data, is deformed by forward models of fault-propagation folding. In the pre-deformed state, the model's GRn2 horizon is tied to its mapped location on the south side of Umtanum Creek. In the final deformed state, the fault tip must lie along the axial plane of the syncline and place the GRr2 horizon near its mapped location. These conditions ultimately constrain the location of the fault tip and the amount of slip.

Fault-bend folding

In addition to fault propagation folding, I consider a flexural slip or fault-bend fold (FBF) (Suppe, 1983) as an alternate kinematic model for the Umtanum anticline. FBFs form in layered sequences through the bending of faulted horizons as they move over non-planar fault surfaces. Major folds in contractional settings form from steps in décollement along thrust faults. Kinematic models of FBF have been applied to many thrust settings (e.g. Suppe, 1983; Abascal, 2005; Madritsch et al., 2008). Casale (2012) kinematically modeled Saddle Mountains anticline, another YFTB structure, as a FBF. A similar model for Umtanum anticline is a possibility worth considering.

Using the new map to constrain the geometry of the fold at the surface, I iteratively forward model the folding in Umtanum Ridge in cross section along the line of section (Plate 1) using Midland Valley's *Move* structural modeling software. This process models the deformation produced by slip on an input fault, whose location is constrained at the surface. In the initial iterations I placed the fault décollement around 10 km below sea level, where Casale (2012) located the deepest detachment in his models of Saddle Mountains anticline. In the early tests it became clear that the flat-to-ramp transition would have to be constrained to lie at depth under the south dipping limb of the anticline. From this initial state, I iteratively adjusted both the depth of the décollement and the shape of the upper portions of fault until I achieved a good match to the observed structure.

The model output (fold form) is compared to the mapped form of unit GRn2 (the uppermost unit in the Grand Ronde Basalt), because the bounding contacts of this unit are exposed in both the south and north limb of the fold. Erosion has removed the younger units from parts of the fold,

and dip data from both younger and older units are relatively rare. Several notable features must be produced in the modeled deformation in order for it to be a plausible representation of the data, or what I consider a good match (Figure 4). First, the south limb of the anticline steepens gradually from the hinge near the crest of the ridge and places the top of GRn2 near its mapped location. Second, the north limb steepens over a shorter distance than the south limb, placing the base of GRn2 near its mapped locations on the north flank of the ridge. Third, near the location where the fault daylights, the fold limb should be near vertical.

Trishear

One feature apparent in the dip data is the curved, rather than kinked, nature of the fold surfaces within Umtanum ridge. While fault-propagation folding produces kinked geometries, trishear fault-propagation folding produces curved folds with variably dipping forelimb anticlines and footwall synclines (Erslev, 1991). In a trishear fold model (Figure 5), fault displacement is transferred to a **tri**angular **shear** zone fixed at the tip of the fault. Trishear kinematic models have been used in contractional settings where faults originating in crystalline basement rocks propagate into and deform overlying sedimentary sequences (e.g. Erslev, 1991; Allmendinger, 1998; Regalla et al., 2010).

A kinematic model of trishear depends on a number of geometric parameters. As the fault slips, the trishear zone and fault tip migrate up-dip according to the propagation-to-slip ratio (*P/S*). Within the trishear zone, the velocity field decreases from the fault slip rate at the zone's hanging wall boundary to zero at the footwall boundary. The concentration factor *c* determines whether the velocity gradient across the trishear zone is linear ($c = 1$) or non-linear (as a function of the power $1/c$).

The geometric relationships of the trishear model of fault-propagation folding permits inverse modeling to determine parameters for the fault slip, angular width of the trishear zone (trishear angle), *P/S*, and the initial location of the fault tip. I use the inverse modeling code of Cardozo in Allmendinger et al. (2011) implemented in Matlab. For a single iteration, the routine runs a trishear model in reverse to retro-deform (in 2-D) a folded-bed geometry, attempting to return the horizon to its initial shape (presumed to be horizontal and approximately planar). The quality of a trishear model run in reverse can be evaluated by how well it restores the folded horizon to a straight line (in two dimensions). The code uses a least-squares linear regression of the restored horizon to evaluate how well the restored horizon compares to a straight line. The "straightness" of the restored profiled is evaluated by a χ^2 objective function. This function compares the restored points of the model to a regression line through the restored points using the sum of the square of the residuals between the two (Figure 6).

This approach is implemented as an inverse model in order evaluate the best-fit combination of slip, trishear angle, *P/S*, and fault tip location. The code uses a gradient based optimization method; given initial parameters, the model searches a predefined range of parameter values looking for a combination which best restores the horizon to a straight line (i.e. has the lowest found value of the objective function). Though the results of the method are prone to getting caught in local minima, it is computationally efficient and completes quickly.

To better characterize how the model traverses the parameter space and to resolve the issue of unrealistic slip values, I simplified Cardozo's model to invert for two rather than four parameters. With the assumption that the mapped fault, daylighting at the surface, is the master reverse/thrust fault, I can constrain the location of the fault tip. The slip parameter can be constrained for a given ramp angle by the structural relief of the hanging wall horizon over the

footwall horizon. To examine a range of possible ramp angles I evaluate five models with ramp angles of 15°, 30°, 45°, 60°, and 75°. The two remaining unconstrained parameters, P/S and trishear angle, are optimized in each of the five models. Three-dimensional plots of these two parameters versus the χ^2 objective function value document the path of each model run through the parameter space from the initial condition to the identified minimum in the χ^2 objective function. These plots (Figure 7) were used to ensure that the optimization traversed an adequate range of the parameter space. Ultimately, the ramp angle with the lowest value for the objective function should represent the preferred model.

I apply this approach to model the hanging wall profile of the GRn2 unit in order to constrain the ramp angle and trishear parameters of the fault. The hanging wall profile was constructed using dip data collected in the field and from lidar and consists of 53 points in the plane of section. The hanging wall profile used in evaluating the FBF model (Figure 4) formed the basis for the new profile used for the trishear modeling. The original FBF profile was resampled at 50 m intervals along its length and manually adjusted in order to produce a profile with smoothly varying dip, as these smoothly varying profiles are characteristic of trishear. Following the example in Allmendinger et al. (2011), only the forelimb part of the folded horizon is used as an input in this model, as this is the region influenced by trishear. Trishear models, in themselves, do not address the formation of fold backlimbs (Figure 8). I will assume that the backlimb of the fold formed due to a flat-to-ramp transition in the fault plane at depth. The depth of the N2 horizon in the footwall is constrained by the geologic map and is considered in this model.

Results

Each of these kinematic approaches yields quite different results for interpreting the structure beneath Umtanum Ridge. The various models produce differences in final fold form, fault form and displacement, and depth to detachment. With these results I can evaluate a range of geometries and their relative strengths and weaknesses.

Fault-propagation folding

I have evaluated the parameter space of possible fault geometries, assuming the Umtanum anticline is a fault propagation fold. The western Umtanum fold geometry can be approximated by either a blind fault (Figure 9A-C) or an emergent fault (Figure 10).

Figure 9 shows the solutions presented for the case of a blind fault, with three dip domains defining the structure (Figure 3). The three solutions presented for the blind case represent both the mean and extremes in the hinge to limb angle γ (and hence the fault cutoff angle θ), representing the range of fold limb dips permissible by the flow-top attitudes presented on the map within 1 km of the line of section. (A), (B), and (C) show mean, maximum, and minimum values, respectively, for the hinge-to-limb angle and the fault cutoff angle or dip. This results in a mean fault dip of 31° with maximum and minimum values of 35° and 28°, respectively (Table 1). In each case the depth to detachment varies from 1800 m (A and C) to 2300 m (B) below sea level, generally near the base of the CRB as inferred from the YM 1-33 borehole. The amount of slip from the detachment ranges from 760 m (A and B) to 910 m (C), based on the dip of the fault and the amount of slip required to generate the observed structural relief on the GRr2 horizon.

Figure 10 presents a model of W Umtanum Ridge as an emergent fault propagation fold. In this case, two dip domains define the structure of the anticline (Figure 3). I present a model with the mean orientations of the two limbs calculated from assumed populations of both forelimb and backlimb flow-top attitude measurements. The mean case results in a fault dip of 31° and 1750 m of slip with a detachment depth of 890 m below sea level (Figure 10). Table 1 contains the hinge-to-limb and fault cutoff angles for all three cases. The maximized and minimized cases only differ superficially from the mean case and are not presented here for this reason.

Fault-bend folding

The results of the iterative forward modeling assuming fault-bend folding is as follows. A steeply dipping fault with the décollement horizon beneath the CRBG can adequately reproduce the observed folding of the GRn2 unit of the CRBG in Umtanum Ridge, meeting most of the specified criteria (Figure 4). The one criterion not met is the near-vertical dip of the northernmost part of the fold. This requirement may not be producible using a fault bend fold algorithm. Folds with steeply dipping forelimbs are more easily produced during fault-propagation fold or may be present due to drag folding of the hanging wall near the fault surface. I address this issue further in the **Discussion** section. The slip required ranges from 440 m to 520 m on a listric fault with a décollement at 4.1 km below sea level. 480 m of slip produces the best fit to the geologic data. As shown in Figure 11, the majority of the modeled fault dips 70° to the southwest. In order to match the moderately north dipping part of the forelimb, the fault must shallow to about 15° before reaching the surface. This method locates the detachment at a depth of 4100 m below sea level, below the CRBG.

Trishear

The most shallowly dipping fault considered by the trishear models seems to best reproduce the shape of the forelimb. Figure 6 shows that the lower the ramp angle, the lower the final value of the objective function (χ^2). The final (best-fit) parameters for each of the five inverse models are shown in Table 2. The trishear model with the lowest objective function for the five ramp angles considered has the following parameters: 15° ramp angle, 4600 m of fault slip, 100 degree trishear angle, and P/S of 1.9. Among these parameters, the value of slip is unreasonably high because the whole fault has a uniform shallow dip. One potential solution is that structural relief is generated from a more steeply dipping fault which transitions to a shallow dip near the surface. I explore this possiblity further in the **Discussion**.

Discussion

The three approaches to modeling produce differing results to the interpretation of fault structure beneath Umtanum Ridge. Each set of results have their limitations in how they compare to the structure and geology observed at Umtanum Ridge. Despite the limitations, it is possible to extract useful information, even with the limited data.

Fault-propagation fold modeling

I do not consider the interpretation of Umtanum anticline as a fault-propagation fold to be very robust; however some approaches result in better reconstructions than others. The Suppean model of fault-propagation folding requires identification of two or three dip domains (Figure 2). Grouping the dip data from Umtanum Ridge into these discrete dip domains is problematic. A visual and statistical analysis of the dip data projected onto the section (Figures 3, 9, 10) shows

that dips vary substantially and do not easily fit into such discrete domains. In particular, the lack of dip data from the center of the fold, due to poor exposure, makes it difficult to distinguish whether there are two or three dip domains. More did data from this part of the fold would help to determine if this FPF approach is an appropriate model.

The two styles of fault-propagation folding, both faulted and unfaulted, produce significantly different geometries for Umtanum anticline. For the following reasons, I prefer the unfaulted case. The few attitudes collected between the more distinct groupings of the moderately dipping southern limb and the steeply dipping forelimb, based on their low dip angles, would seem to suggest the presence of three dip domains, supporting the unfaulted interpretation. In contrast, these shallowly dipping attitudes are difficult to reconcile within the two dip domains of the faulted case. Also, in contrast to the blind case, the emergent case requires a relatively shallow detachment depth, well within the CRBG, which would seem unlikely due to the inference of paleostructural relief from thickness variations in the CRBG at other YFTB structures (Reidel, 1984).

If the geometry of Umtanum anticline is better represented by the unfaulted case, what accounts for the thrust mapped at surface? I propose that the mapped fault represents a synclinal breakthrough from propagating fault to the surface. This phenomena is observed in fault-propagation folds where the fault tip encounters layers that are unable to fold, due to bending resistance, into the tight anticline above the propagating fault surface (e.g. Suppe and Medwedeff, 1990). In such cases, the fault breaks through either the axial surfaces of the anticline or syncline, or the steep limb of the fold. The mapped disposition of the unit contacts and the flow-top attitudes support the synclinal breakthrough option. Based on the horizons offset by the mapped fault, a maximum of 150 m slip can be inferred from the breakthrough

event. This slip would be included in the slip magnitudes presented in the **Results** section, because slip from both the breakthrough and incremental fault-propagation would generate structural relief on the horizon (GRr2) I used to determine fault position and slip.

There are a few assumptions inherent to the modeling approaches used in this study. The modeled slip has occurred post-emplacement of unit GRr2 because both the slip and position of the fault are required to match the observed contact positions of the top of unit GRr2. This assumption differs from the observation at other YFTB structures that CRBG flows were emplaced syntectonically with anticlinal growth (Reidel, 1984). Another assumption is that the modeling software requires a stratigraphy that does not vary in thickness. The stratigraphy recorded in borehole YM 1-33 forms the basis for the model stratigraphy, representing a minimum thickness assuming the existence of paleostructural relief and syntectonic emplacement of CRBG flows, as YM 1-33 drilled the hinge of the southern anticline. This results in the apparent problem with the model cross sections where the unit contacts other than GRr2 do not line up with their mapped positions. The problem can be solved if one assumes that the CRBG flow units thicken into the synclinal troughs, as would be expected if they were emplaced syntectonically.

Ultimately, a fault-propagation fold producing three distinct fold limbs with a synclinal breakthrough is my preferred model among all of the fault-propagation fold models (Figure 9). With the master-fault detachment located near the inferred base of the CRB, this model suggests a thin-skinned origin for Umtanum ridge. The main drawback to this interpretation is that it fails to explain all of the observed flow-top attitudes, which appear to vary more smoothly than in a kinked-fold model.

Fault-bend fold modeling

The fault-bend fold modeling I performed sought to reproduce the form of Umtanum anticline solely via changes in the dip of the fault. With the freedom to modify fault shape with very few constrains, a fold form that closely honors the attitude data was achieved. Comparing Figures 4 and 11, most of the fold form produced via forward modeling matches the observed form, including total structural relief, the southern limb form, and the smooth transition of the attitudes from south dipping limb to the northern limb. The steeply dipping portion of the fault generates the observed structural relief. Both listric bends produce different portions of the fold, the lower bend producing the moderate dip of the south-dipping back limb and the upper bend producing the gently dipping part of the forelimb.

The northernmost, steeply dipping, portion of the fold is not reproduced with this model. Figure 11 shows that observed dips in the northernmost part forelimb of the anticline are steeper than any dips modeled using movement on the modeled fault. I surmise that this discrepancy exists because of a slip gradient, where the amount of fault slip decreases towards the surface, and shortening is accommodated by folding of the CRBG rocks. About 110 m of slip appears to be taken up by folding near where the fault daylights, based on the observed versus modeled form of unit GRn2. The most likely explanation is that slip is transferred to fault-propagation folding through either the Suppean style or trishear. Such a situation is investigated later in the **Synthesis of interpretations** section.

The depth of faulting implied from this fault-bend fold model has implications for the thick vs thin-skinned debate. The décollement depth at about 4 km below sea level would put the depth of faulting into the Paleogene sedimentary section, specifically into the Swauk Formation as

interpreted by Campbell (1989) in the YM 1-33 borehole. This borehole bottomed out only 300 m deeper than the modeled depth of the detachment and did not penetrate any crystalline rocks. Inversion of the geophysical data suggests crystalline basement may exist close to this depth, so although speculative, I cannot rule out basement involvement in the overall fault structure. The borehole dip log shows folding in the Paleogene sedimentary rocks and it is tempting to attribute this folding to deep faults similar to the one modeled. Other possible explanations for this folding include Eocene age syn-extensional sedimentation in fault-bounded grabens (Johnson, 1985; Evans, 1994) or, alternatively, deposition in synclinal basins between reverse faults (Cheney and Hayman, 2009). Ultimately, it is difficult to connect deformation at deeper crustal levels to the surface deformation with limited data; however, the ability of a deep-going fault to closely model the surface deformation is intriguing.

Trishear

The inverse modeling of trishear attempted to reproduce the forelimb fold form of Umtanum anticline. The results of the five test of different ramp angles showed that more shallowly dipping faults produce folds with a better match, as measured by the χ^2 objective function, to the observed forelimb. This was made possible by reducing the number of free parameters in Cardozo's trishear inverse code, allowing for a simple analysis of how the inverse model traverses the parameter space. This assures that an adequate range of parameters are tested and that the model doesn't get caught in unrealistic local minima. Figure 7 shows the values of the modeled parameters (P/S and trishear angle) and the objective function at each iteration of the model for five different ramp angles. The plots show that, for each ramp angle, the model traverses a wide range of reasonable values for P/S and trishear angle. This analysis gives me confidence in the model's final output of trishear parameters.

Applying Cardozo's method of trishear inverse modeling to Umtanum ridge is hamstrung by the lack of subsurface data at Umtanum ridge. Without data resolving multiple offset horizons at depth, it is difficult to place narrow bounds on the possible ranges of values for the trishear parameters (slip, trishear angle, *P/S*, and fault tip location). Initial tests of the inverse model using the four bounded parameters yield results with low χ^2 objective function values; however, it was not clear if the model was testing an adequate range of the parameter space. In the case of the slip parameter, the model consistently chose a value of slip equal to the value of the upper bounds, even if the bound was set unrealistically high. Due to these challenges I sought to reduce the number of variable parameters.

The reduction in freely varying parameters, from the four parameters in Cardozo in Allmendinger (2011) to two parameters, relies on two assumptions; the first of these assumptions, taken as one of the fixed parameters in the model, is the final location of the fault tip. For this modeling I assume that the intersection of the mapped fault on the north side of Umtanum ridge and the line of section is the tip of the fault responsible for trishear deformation. The fault-propagation fold case considers the possibility of a blind fault controlling the deformation, with the mapped fault representing a synclinal breakthrough. A similar situation is possible in the trishear case; however, modeling this situation is impractical because of the lack of subsurface data leaves no constraints on the likely position of a blind fault tip. The second assumption concerns the amount of slip. A fixed slip parameter is used for each modeled ramp angle. Again, this assumption was made in order to reduce the number of free parameters. The amount of slip is that which is necessary to produce the observed structural relief of the hanging wall input horizon above the footwall horizon. This results in five values of slip corresponding to the five ramp angles (Table 2). One drawback to this method is that it requires unrealistically

high magnitudes of slip for the low ramp angle models (e.g. 4600 m for the 15° ramp angle). Considering the results of the fault-bend fold modeling, it seems reasonable to assume that structural relief could be produced by a significantly lower magnitude of slip on a more steeply dipping portion of the fault. In this case, the part of the fold with greatest curvature near where the fault daylights, which could not be reproduced using fault-bend folding, could be seen as having been formed by trishear fault-propagation folding as the fault broke the surface. I examine this hybrid model more closely in the following section.

Synthesis of interpretations

The kinematic modeling produced a variety of results, but which method best reproduces the observed deformation at Umtantum Ridge? The methods produce contrasting fold styles: kinked folds, in the fault-propagation models and more curved folds, in the fault-bend and trishear models. The available dip data seem to support the curved fold models; however, due to the relative dearth of data from the middle part of the fold I cannot conclusively rule out the blind FPF case (Figure 9). The fault-bend fold model (Figure 11) honors all of the dip data except for at the northernmost part of the hanging wall. This part of the fold is best reproduced using a trishear model.

I propose a hybrid model, combining parts of the fault-bend fold and trishear model, best explains the formation of Umtanum Ridge. The backlimb and structural relief are likely the product of the more steeply dipping portion of the fault which bends upward from a deep detachment. The forelimb part could have then formed where the fault shallows and propagates to the surface. The best evidence for such an arrangement is that both the trishear and fault-bend fold models favor a relatively shallow fault ramp angle where the fault daylights. Using this 15°

ramp angle from the trishear modeling coupled with the 110 m of excess slip at the shallowest part of the fault in the fault-bend fold model I can test this hybrid model in *Move* using a trishear forward model on top of the fault-bend fold model. After running the fault-bend fold model in Figure 11, minus 110 m of slip, to begin forming the anticline (Figure 12A), I iteratively ran forward models of trishear on the fold form, attempting to produce the overturning observed in the northernmost part of the fold. I used 110 m of slip with the trishear zone migrating up the shallowly dipping portion of the fault constructed for fault-bend folding. The best result used a propagation/slip ratio of 5 and a trishear angle of 90°. The result (Figure 12B) shows that overturning of the forelimb can be accomplished by trishear following fault-bend folding. The modeled fold form is not an exact match to the observed but I am confident that this could be refined with furture work.

Implications

Depending on the kinematic model used, Umtanum anticline can be reproduced with faults that fit into either the thick or thin-skinned paradigms. In the model I favor, the hybrid trishear/fault-bend fold model, faulting clearly penetrates the CRBG suggesting a thick-skinned interpretation. The best model of fault-propagation folding would indicate a thin-skinned interpretation but this is not supported by all of the dip data. Detailed study of structural geometry and strain distribution within Umtanum anticline to the east of the study area, near the Columbia River at Priest Rapids Dam, produced results that are ambiguous with regard to the thick versus thin-skinned question (Price, 1982; Price and Watkinson, 1989). Their analysis suggests that the daylighting Umtanam thrust/reverse fault at this locality formed relatively late during fold development out of the kinked fold at depth. This conclusion relates to the western Umtanum anticline, in this study's field area, in two ways. First, that their analysis suggests a kinked

geometry at depth would support some notion of fault-propagation folding from a structure originating at indeterminate depth, which does not conclusively favor one model over the other. Second, that the uppermost portion of the Umtanum fault has formed late in the development of the anticline and at a shallower dip than the deeper structure is similar to this study's hybrid fault-bend trishear model.

Deeper structure beneath Umtanum ridge is hinted at in the geophysical data from the region. A two-dimensional crustal model generated from the inversion of aeromagnetic and gravity data proposes that the faults under Umtanum Ridge cut deeply into the pre-Paleogene crystalline basement (Blakely et al., 2011). The fault-bend/hybrid model presented here does not preclude this possibility. The detachment is located near the pre-Paleogene basement of the geophysical crustal model and the maximum depth penetrated by well YM 1-33, which bottomed out in Paleogene sedimentary rocks (Campbell, 1989). The relief, implied by the geophysical data, on the basement-sedimentary interface could have formed during erosion; Paleogene extension (Catchings and Mooney, 1988; Evans, 1994); or alternatively, Paleogene shortening (Cheney and Hayman, 2009). Casale (2012) found that tapered bedding, imaged seismically in sub-CRBG clastic rocks under Saddle Mts. anticline, indicates onlapping on a growing anticlinal structure, implying shortening in the YTFB dating to late Eocene time. Speculatively, the south-dipping clastic rocks known from the dip log of the YM 1-33 borehole through Umtanum Ridge South could have an analogous relationship to CRBG deformation at Umtanum Ridge. Interpretations of the seismic reflection data under Saddle Mts. point to the presence of at least one deep fault (Casale, 2012), similar to the fault-bend/hybrid model at Umtanum Ridge.

Assuming the hybrid fault model best represents the cause of deformation at Umtanum Ridge, I can estimate the implied rate of slip and compare that to other estimates from the region.

Because the cross sections show shortening only in the plane of the section, these slip rate and strain estimates are inherently two-dimensional, addressing deformation only within the plane of the section. The total amount of slip since the emplacement of the Grande Ronde basalt at 15.6 Ma (Reidel et al. 1989b) gives average slip rates over that interval. Total slip on the model fault (given by the modeled slip required to reasonably approximate the geometry of the anticline) gives a value of 440 to 520 m, to give an average slip rate of 0.028 mm/yr to 0.033 mm/yr.

In order to compare shortening accommodated by Umtanum ridge to observed geodetic rates from GPS, I consider the total heave accrued since Grande Ronde emplacement on the modeled fault. (Heave is the horizontal component of the total slip.) Using fault heave gives horizontal shortening rates of 0.009 to 0.012 mm/yr. McCaffery and others (2013) calculated strain rates in the Yakima folds from the regional GPS velocity field. They found a N-S directed strain rate of -4.1±0.1 ns/yr along a transect near the Yakima canyon. This strain rate predicts a N-S horizontal shortening rate of 0.02 mm/yr across the 5 km breadth of Umtanum Ridge. This value of shortening rate is taken as a minimum because of the 34° discrepancy between the presumed transport direction and the N-S trending transect from McCaffery et al. (2013). The geodetically derived shortening rate is of the same order of magnitude but about twice as large as the estimate derived from the kinematics of Umtanum Ridge alone. I surmise that the difference between the GPS observations and the kinematic reconstruction can be attributed to shortening on other structures, such as the south vergent thrust fault east of Yakima Canyon, or that slip may be accommodated on the adjacent folds (Manashtash and Umtanum Ridge South) in the region. An alternative explanation is that GPS derived shorting rates have sampled a modern rate that is roughly twice the geologic average.

In addition to horizontal shortening, I can evaluate the vertical uplift rate implied by the kinematic model. Based on the amount of throw (the vertical component of total slip) determined from fault slip in the fault-bend/hybrid kinematic model, uplift rates range from 0.026 mm/yr to 0.031 mm/yr. Between 640 and 880 m of total structural relief has been produced on the GRn2 horizon at the line of section. The minimum is taken as the difference in elevation between the crest of Umtanum Ridge, where unit GRn2 is exposed, and the projected elevation of the top of the same unit based on its dip and position in the footwall. Since unit GRn2 has likely been eroded from the crest of the ridge, the maximum structural relief is calculated by adding the thickness of unit GRn2 as is exposed in Yakima Canyon at Umtanum Ridge South. The uplift rate implied by structural relief since Grande Ronde time (15.6 Ma) is between 0.041 and 0.056 mm/yr. Because these rates are higher than the rates derived from kinematic modeling it is possible that other structures beneath Umtanum Ridge are helping to produce structural relief. Such structures could either be local to Umtanum Ridge (e.g. conjugate faults) or could extent to adjacent folds (e.g. Manastash), generated structural relief across a larger region. For comparison with structural relief, total topographic relief at the line of section is about 600 m from the Yakima River to the crest of the ridge. Because the structural relief on the ridge-top unit is at least 640 m, this implies at least 40 m of erosion at the crest. There could be much more erosion if younger units were ever emplaced over the ridge crest. It is not clear if flow units younger than GRn2 overtopped Umtanum Ridge on the west side of the Yakima River, but they do on the east side just outside of the map area. These younger flows, if eroded from the western end of the ridge, would represent about 10 m of additional erosion. To the north of the map area at Manastash Ridge an uplift rate of 0.17 mm/yr was inferred over the last 4 My (Ladinski, 2012) based on luminescence dating of strath terraces in the hanging wall of the

Manastash anticline. This higher rate at Manastash could imply that the uplift rates in the region are higher in more recent times, or that rates are simply higher at Manstash Ridge than at Umtanum Ridge.

Umtanum Ridge lies along the enigmatic Olympic-Wallowa Lineament (OWL), a possibly tectonic feature first identified on geomorphic maps (Raisz, 1945) which extends from the Olympic Peninsula, across the Cascade Range and Columbia Basin, and into northeast Oregon. It has been postulated that the OWL represents a major crustal structure accommodating contraction (McCaffrey et al., 2007 and 2013, Blakely et al. 2011) and/or dextral shear (*e.g.* Wise, 1963; Hooper and Conrey, 1989; Pratt, 2012). Geophysical data suggest that the OWL connects the active faults in the Puget Lowland to the structures of the YFTB (Blakely et al., 2011). One hypothesis is that the OWL is a major strike-slip fault system with the Yakima folds representing splay faults connecting to the OWL at mid to lower crustal levels (Pratt, 2012).

The result of the fault-bend kinematic modeling indicates that faulting could extend into at least the middle crust below the OWL at Umtanum Ridge. This result does not preclude the linking of the Umtanum fault to a deeper structure, such as an OWL related strike-slip fault; however, this study found no direct evidence for strike-slip at this locality. The structure is kinematically restorable using only reverse-sense motion, but this is unsurprising since I only looked at structure from two dimensions. Additional kinematic models along the trend of the anticline could be used to evaluate the presence or absence of strike-slip in the middle to upper crust.

Future work

Because this study relies on only one line of section, my preferred interpretation of Umtanum Ridge as a fault-bend/trishear related fold requires more testing before I can confidently declare

it valid. My confidence would be bolstered if additional kinematic models along strike showed similar reconstructions and slip magnitudes. The mapping completed for this project could serve as the basis for future kinematic modeling. Improving individual kinematic reconstruction requires additional data on the subsurface structure. Subsurface structure could be imaged seismically, although seismic imaging of the GRBG and underlying rocks is difficult because of low impedance contrasts between the CRBG flows. Seismic imaging was successful at Saddle Mts. (Casale, 2012) and perhaps new campaigns could have similar success at Umtanum Ridge. The precise earthquake locations could also illuminate subsurface structure. The best interpretation to date, based on the existing seismic network, is that seismicity in the YFTB is diffuse and not correlated to mapped structures (Gomberg, et al., 2012). Earthquake locations could be better constrained using a dense temporary seismic array deployed across structures of interest (e.g. Drew et al., 2013; Meighan et al., 2013). If earthquakes are localized onto planar surfaces they could conceivably define fault structure at depth.

Conclusions

I present previously unpublished mapping and incorporate interpretation of high resolution lidar DEMs to extract useful structural data from Miocene CRBG flows in the area surrounding the intersection of Umtanum Ridge and Yakima Canyon. Using this data to constrain the geometry of the anticline comprising Umtanum Ridge along a line of section, I employ three kinematic models to investigate how fold form relates to fault form at depth beneath the structure. The results of the kinematic modeling reveal that Umtanum Ridge is best explained by a steeply dipping fault extending beneath the CRBG and into Paleogene sedimentary rocks. This modeling includes “thin-skinned” interpretations which may plausibly explain the fold form at Umtanum Ridge; however, the structural data show a noticeable bias towards a “thick-skinned”

interpretation. Such an interpretation, if correct, would imply that the seismic hazard posed by Umtanum Ridge, and perhaps other YFTB structural analogs, tends towards the upper end of previous estimates.

In the broader tectonic picture, middle-Miocene-to-present deformation rates derived from my preferred kinematic model underestimate the rates derived from geodetic and geomorphic data. This may suggest greater activity in more recently in this part of the YFTB or that deformation at Umtanum Ridge is not representative of the region. In any case, these models are primarily based on surficial data and are largely unconstrained in the subsurface. Further work is necessary, especially the acquisition of higher resolution subsurface data, in order to test the kinematic models I present here.

References

Abascal, L.V., 2005, Combined thin-skinned and thick-skinned deformation in the central Andean foreland of northwestern Argentina: Journal of South American Earth Sciences, v. 19, p. 75-81.

Allmendinger, R.W., 1998, Inverse and forward numerical modeling of trishear fault-propagation folds: Tectonics, v. 17, p. 640-656.

Allmendinger, R.W., and Shaw, J.H., 2000, Estimation of fault propagation distance from fold shape: Implications for earthquake hazard assessment: Geology, v. 28, p. 1099-1102.

Allmendinger, R.W., Cardozo, N., and Fisher, D.M., 2012, Structural Geology Algorithms, New York: Cambridge University Press, 289 pp.

Benjamin & Associates, URS Corporation, Geomatrix Consultants, and Shannon & Wilson, 2012, Probabilistic seismic hazard analyses project for the mid-Columbia dams (Prepared for Public Utilities Districts of Chelan, Douglas, and Grant Counties), 344 pp.

Bentley R.D., 1977, Stratigraphy of the Yakima basalts and structural evolution of the Yakima Ridges in the western Columbia Plateau. *In:* E. H. Brown & R. C. Ellis *eds.* Geology excursions in the Pacific Northwest. Bellingham: Western Washington University, p. 339-389.

Blakely, R.J., Sherrod, B.L., Weaver, C.S., Wells, R.E., Rohay, A.C., Barnett, E.A., and Knepprath, N.E., 2011, Connecting the Yakima fold and thrust belt to active faults in the Puget Lowland, Washington: Journal of Geophysical Research, v. 116, p. B07105. doi: 10.1029/2010JB008091

Bruhn R.L., 1981, Preliminary analysis of deformation in part of the Yakima fold belt, south-central Washington. Richland, Washington: Washington Public Power Supply System Report, 27 p. *(as reported by Watters, 1989).*

Calabró, R.A., Corrado, S., Di Bucci, D., Robustini, P., and Tornaghi, M., 2003, Think-skinned vs. thick-skinned tectonics in the Matese Massif, Central—Southern Apennines (Italy): Tectonophysics, v. 377, p. 269-297.

Campbell, N.P., and Bentley, R.D., 1981, Late Quaternary deformation of the Toppenish Ridge uplift in south-central Washington: Geology, v. 9, 519-524.

Campbell, N.P., 1989, Structural and stratigraphic interpretation of rocks under the Yakima fold belt, Columbia Basin, based on recent surface mapping and well data. *In:* S.P. Reidel and

P.R. Hooper, *eds.* Volcanism and Tectonism in the Columbia River Basalt Province. Geological Society of America Special Paper 239, p. 209-222

Casale, G.M., 2012, Core complex exhumation in peri-Adriatic extension, and kinematics of Neogene slip along the Saddle Mountains thrust [Ph.D. Dissertation]: Seattle, University of Washington, 85 p.

Catchings, R., and Mooney, W., 1988, Crustal structure of the Columbia Plateau: Evidence for continental rifting: Journal of Geophysical Research, v. 93, p. 459-474.

Cheney, E.S., and Hayman, N., 2009, The Chiwaukum Structural Low: Cenozoic shortening of the central Cascade Range, Washington State, USA: Geological Society of America Bulletin, v. 121, p. 1135-1153.

Drew, J., White, R.S., Tilmann, F., and Tarasewicz, J., Coalescence microseismic mapping: Geophysical Journal International, v. 195, p. 1773-1785.

Erslev, E.A., 1991, Trishear fault-propagation folding: Geology, v. 19, p. 617-620.

Evans, J.E., 1994, Depositional history of the Eocene Chumstick Formation: Implications of tectonic partitioning for the history of the Leavenworth and Entiat-Eagle Creek fault systems, Washington: Tectonics, v. 13, p. 1425-1444.

Fisher, N. I., Lewis, T. L., and Embleton, B. J., 1987, Statistical analysis of spherical data: Cambridge, Cambridge University Press, 329 p.

Geomatrix Consultants, 1996, Probabalistic seismic hazard analysis DOE Hanford site, Washington, WHC-SD-W236A-TI-002, Rev. 1, 372 pp.

Gomberg, J., Sherrod, B., Trautman, M., Burns, E., Snyder, D., 2012, Contemporary Seismicity in and around the Yakima Fold-and-Thrust Belt in Eastern Washington, Bulletin of the Seismological Society of America 102:309-320; doi:10.1785/0120110065

Goff, F., 1981, Preliminary geology of eastern Umtanum Ridge, south-central Washington, Rockwell International, Rockwell Hanford Operations, Energy Systems Group.

Hagood, M.C., 1986, Structure and evolution of the Horse Heaven Hills in south-central Washington, Basalt Waste Isolation Program, Rockwell International, Rockwell Hanford Operations.

Hooper, P.R., and Conrey, R.M., 1989, A model for the tectonic setting of the Columbia River basalt eruptions. *In:* Reidel, S.P. and Hooper, P.R., Volcanism and tectonism in the Columbia River flood-basalt province, Geological Society of America Special Paper, v. 239, p. 293--306.

Johnson, S.Y., 1985, Eocene strike-slip faulting and basin formation in Washington: AAPG Bulletin, v. 68, p. 493.

Madritsch, H., Schmid, S.M., and Fabbri, O., 2008, Interations between thin- and thick-skinned tectonics at the northwestern front of the Jura fold-and-thrust belt (eastern France): Tectonics, v. 27, p. TC5005.

Mazzotti, S., Dragert, H., Hyndaman, R.D., Miller, M.M., and Henton, J.A., 2002, GPS deformation in a region of high crustal seismicity: N. Cascadia forearc: Earth and Planetary Science Letters, v. 198, p. 41-48.

McCaffrey, R., Long, M.D., Goldfinger, C., Zwick, P.C., Nabelek, J.L., Johnson, C.K., and Smith, C., 2000, Rotation and plate locking at the southern Cascadia subduction zone: Geophys. Res. Lett., v. 27, p. 3117-3120.

McCaffrey R, A I Qamar, R W King, R Wells, G Khazaradze, C A Williams, C W Stevens, J J Vollick, P C Zwick, 2007, Fault locking, block rotation, and crustal deformation in the Pacific Northwest. Geophysical Journal International v. 169, p. 1315-1340.

McCaffrey, R, R. King, SJ Payne, M Lancaster, 2013, Active tectonics of northwestern U.S. inferred from GPS-derived surface velocities, J. Geophys. Res. Solid Earth, 118, 709–723, doi:10.1029/2012JB009473.

Meighan, L.N., Cassidy, J.F., Mazzotti, Stephane, and Pavlis, G.L., 2013, Microseismicity and tectonics of southwest Yukon Territory, Canada, using a local dense seismic array: Bulletin of the Seismological Society of America, v. 103, p. 3341-3349.

Mitra S, 1990, Fault propagation folds: geometry, kinematics evolution, and hydrocarbon traps. AAPG Bulletin v. 74, p. 921-945

Pratt, T.L., Large-scale splay faults on a strike-slip fault system: The Yakima Folds, Washington State: Geochemistry, Geophysics, Geosystems, v. 13, p. Q11004.

Price, E.H., 1982, Structural geometry, strain distribution, and mechanical evolution of eastern Umtanum Ridge and a comparison with other selected localities within Yakima Fold structures, south-central Washington [Ph.D. Dissertation]: Pullman, Washington State University, 196 p.

Price, E.H., and Watkinson, A.J., 1989, Structural geometry and strain distribution within eastern Umtanum fold ridge, couth-central Washington, *In:* Reidel, S.P. and P.R. Hooper, P.R., Volcanism and tectonism in the Columbia River flood-basalt province, Geological Society of America Special Paper, v. 239, p. 265–281.

Puget Sound Lidar Consortium, 2010, Status of Puget Sound Lidar Consortium Survey November 2010, http://pugetsoundlidar.ess.washington.edu/

Raisz, E., 1945, The Olympic-Wallowa lineament. American Journal of Science: v. 243-A, p. 479-485.

Regalla, C., Fisher, D., and Kirby, E., 2010, Timing and magnitude of shortening within the inner fore arc of the Japan Trench: Journal of Geophysical Research, v. 115, p. B03411.

Reidel, S.P., 1984, The Saddle Mountains; the evolution of an anticline in the Yakima fold belt: American Journal of Science, v. 284, p. 942-978

Reidel, S.P., Fecht, K.R., Hagood, M.C., and Tolan, T.L., 1989a, The geologic evolution of the central Columbia Plateau, *in* Reidel, S.P. and P.R. Hooper, P.R., Volcanism and tectonism in the Columbia River flood-basalt province, Geological Society of America Special Paper, v. 239, p. 247–264.

Reidel S P, P R Hooper, M H Beeson, K R Fecht, R D Bentley, J L Anderson, 1989b, The Grande Ronde Basalt, Columbia River Basalt Group; Stratigraphic descriptions and correlations in Washington, Oregon, and Idaho. *In:* S P Reidel and P R Hooper, *eds.* Volcanism and Tectonism in the Columbia River Basalt Province. Geological Society of America Special Paper 239, p. 21-53

Rowan, M.G., and Linares, R., 2000, Fold-evolution matrices and axial-surface analysis of fault-bend folds: application to the Medina anticline, Eastern Cordillera, Colombia: AAPG Bulletin, v. 84, p. 741-764.

Saltus, R.W., 1993, Upper-crustal structure beneath the Columbia River Basalt Group, Washington: Gravity interpretation controlled by borehole and seismic studies, Geol. Soc. Am. Bull., *105*, 1247–1259.

Schuster, J.E. (compiler), Geologic map of the east half of the Yakima 1:100,000 quadrangle, Washington, 1994. 1 sheet, scale 1:100,000, with 22 p. text.

Suppe, J., 1983, Geometry and kinematics of fault-bend folding: American Journal of Science, v. 283, p. 684-721.

Suppe, J., 1985, Principles of Structural Geology, Englewood Cliffs, New Jersey: Prentice-Hall, Inc., 537 pp.

Suppe, J. and Medwedeff, D.A., 1990, Geometry and kinematics of fault-propagation folding: Ecolage Geolgicae Helvetiae, v. 83, p. 409-454.

Watters T R, 1988, Wrinkle ridge assemblages on the terrestrial planets. Journal of Geophysical Research, 93, 10235-10254.

West M W, F X Ashland, A J Busacca, G W Berger, M E Shaffer, 1996, Late Quaternary deformation, Saddle Mountains anticline, south-central Washington. Geology, v. 24, p. 1123-1126.

Wilkerson, S. M., Apotria, T., and Farid, T., 2002, Interpreting the geologic map expression of contractional fault-related fold terminations: lateral/oblique ramps versus displacement gradients: Journal of Structural Geology, v. 24, p. 593-607.

Wise, D.U., 1963, An outrageous hypothesis for the tectonic patterns of the North American Cordillera: Geological Society of America Bulletin, v. 74, p. 357-362.

Tables

Table 1. Interlimb angles (γ/γ^*) and fault-cutoff angles (θ) for fault-propagation fold models. See text for discussion.

Case	γ/γ^*	θ
Faulted, max interlimb angle	44°	38°
Faulted, mean interlimb angle	38°	32°
Faulted, min interlimb angle	34°	26°
Unfaulted, max interlimb angle	60°	35°
Unfaulted, mean interlimb angle	55°	31°
Unfaulted, min interlimb angle	43°	22°

Table 2. Parameters used in trishear inverse modeling. Trishear angle and P/S are the free parameters the model inverts for. χ^2 is the final value of the objective function. See text for explanation.

Ramp angle	Slip (m)	Trishear angle	P/S	χ^2
15°	4600	100°	1.9	56318
30°	2000	140°	2.4	173632
45°	1300	150°	2.3	464077
60°	1100	160°	1.8	1860447
75°	930	170°	1.0	8139042

Figures

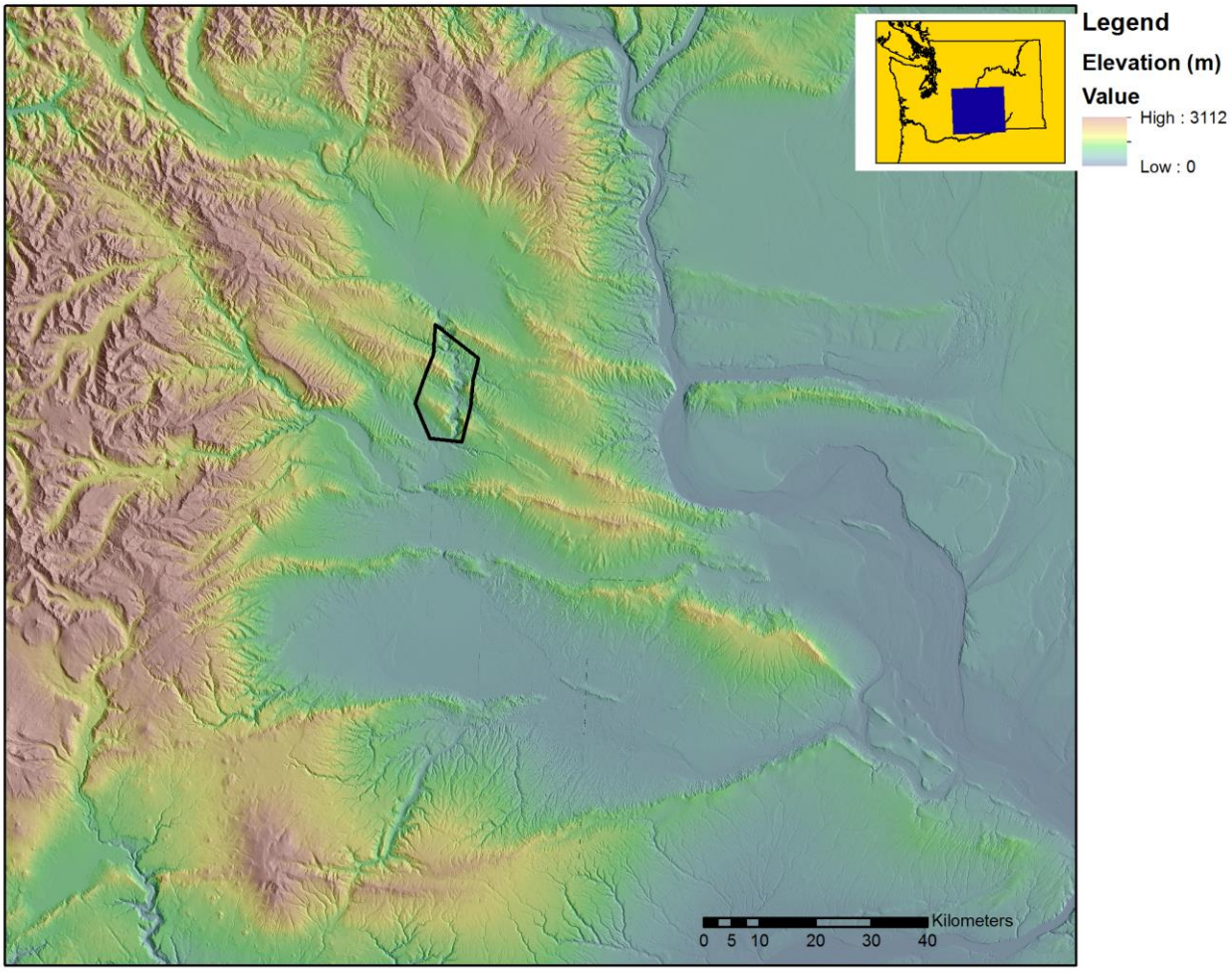

Figure 1. Shaded relief map showing the location of the Yakima fold and thrust belt within Washington. The geologic map in Plate 1 is outlined in black.

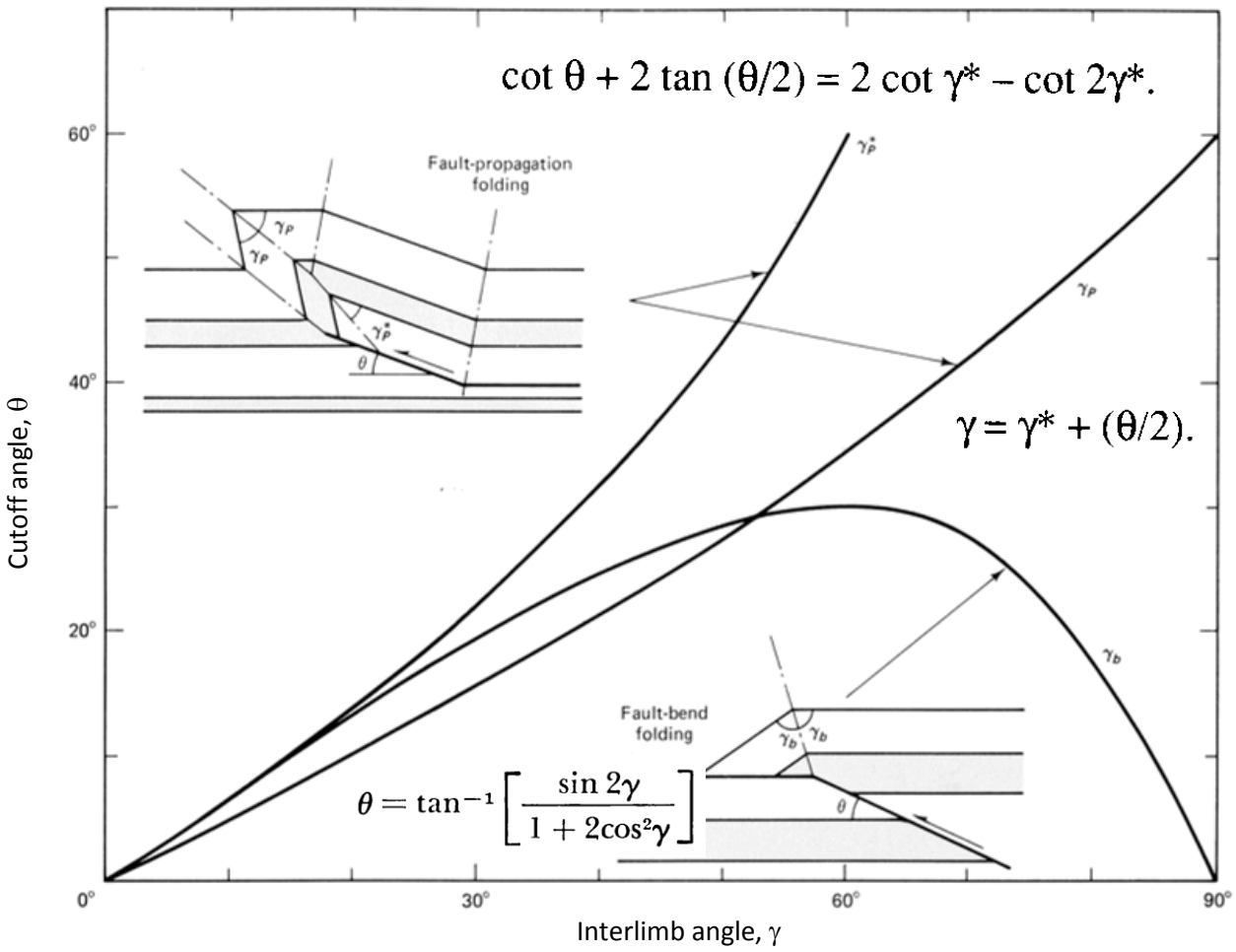

Figure 2. Figure adapted from Suppe (1985) showing geometric relationship between fault-cutoff angle (θ) and interlimb angle (γ) for fault-propagation and fault-bend folds.

Figure 3. Line of section shown at greater scale than in Plate 1. Bold dashed lines denote domain boundaries between anticline fold limbs for both faulted (left) and unfaulted (right) fault-propagation folds. Also shown are equal-area plots of poles to flow-tops in each dip domain. The flow top attitudes are from within 1 km of the line of section and have been corrected for apparent dip with respect to the section line. Bold square and solid angle (encircled area) represent the Fisher mean vector of the poles and alpha-95 cone of confidence, respectively. See Plate 1 for explanation of map symbology.

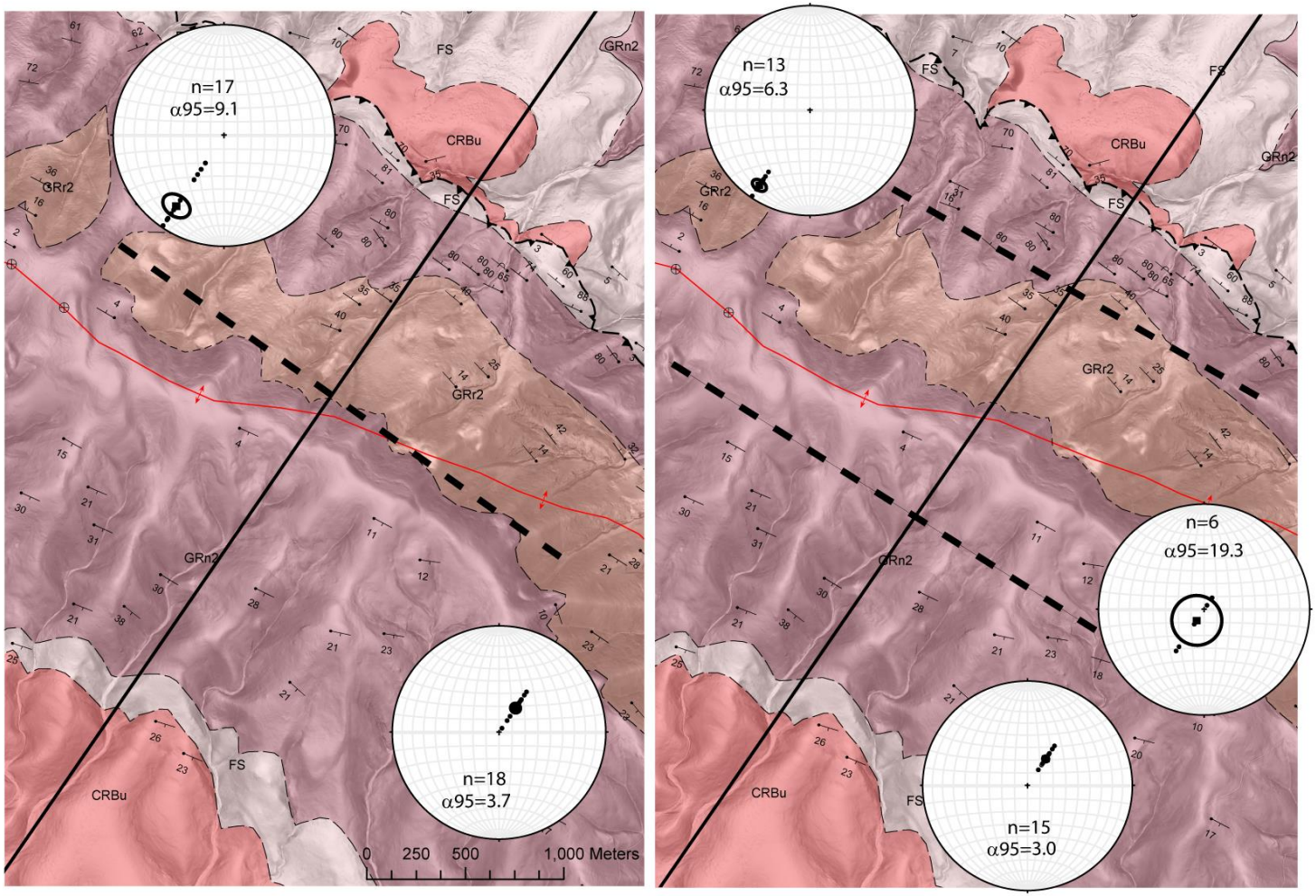

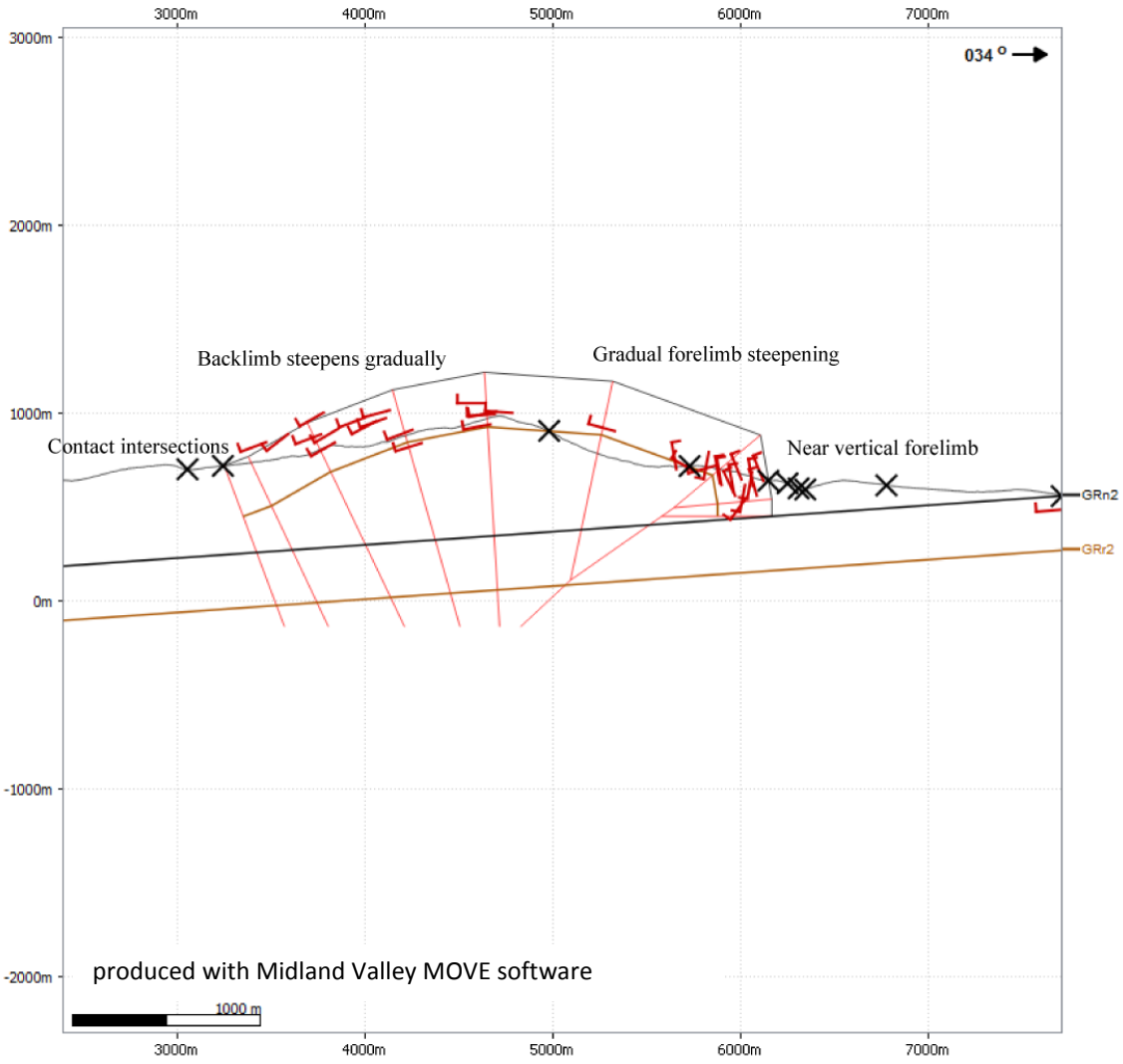

Figure 4. Cross section showing shape of the uppermost unit of the Grand Ronde Basalt (top of unit GRn2 represented by black line) annotated with the criteria to be reproduced via kinematic modeling. The lines below the topographic profile represent the pre-deformed state, inferred from the geometry in the footwall. Dip data from within 1 km of the line of section are displayed as red symbols. Black crosses represent contact intersections with topography. Vertical datum is sea level. Horizontal datum is meters from the southwest end of the line of section (see Plate 1).

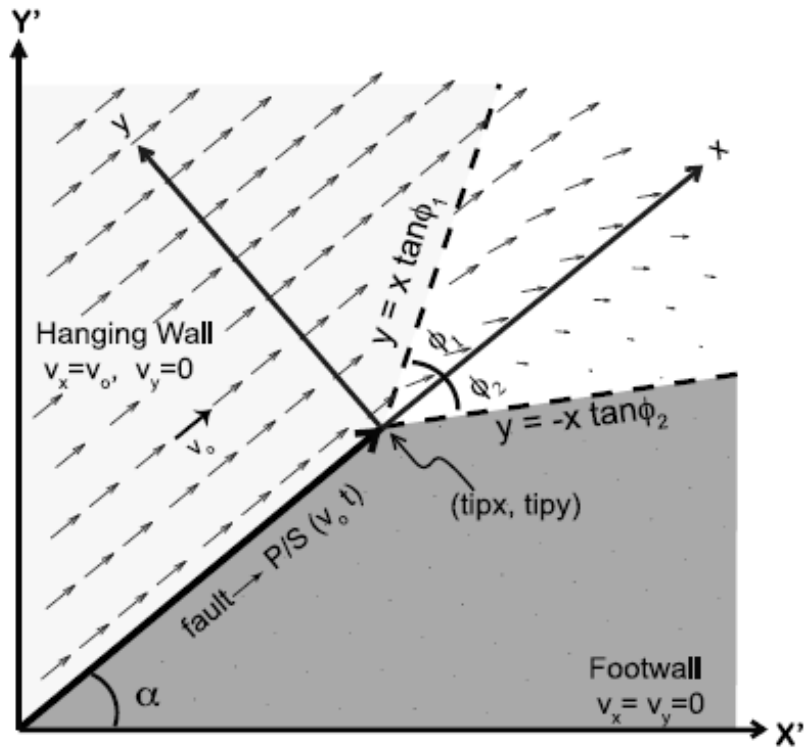

Figure 5. Schematic of trishear fault-propagation folding from Regalla and others (2010). See text for discussion.

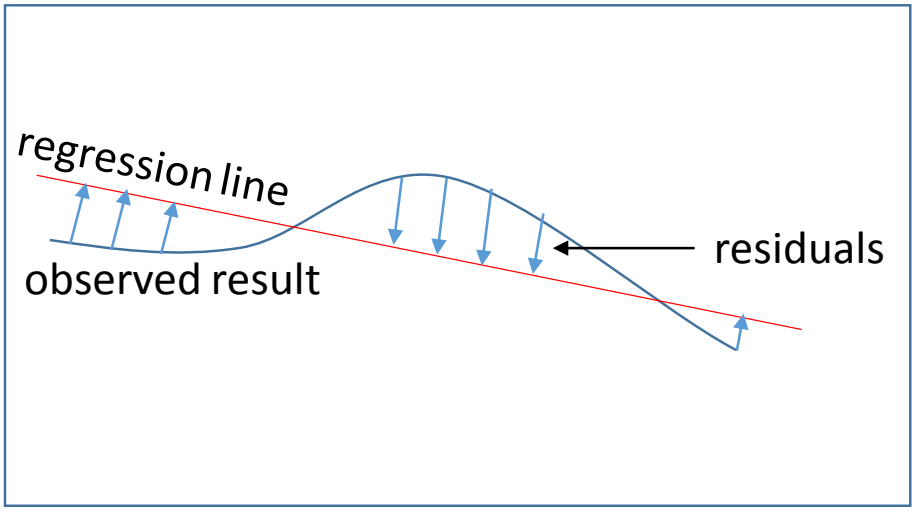

Figure 6. The χ^2 statistic measures the difference between an expected and observed result. In a trishear inverse model, the expected result would be a simple unfolded horizon, or a straight line in two-dimensions. To do this the code fits a regression line through the result of the inversion and computes the sum of the square of the residuals, or distance between the points in the modeled horizon and a regression line fit to the points. The more closely the modeled horizon resembles the regression line, the lowere the value of χ^2 will be.

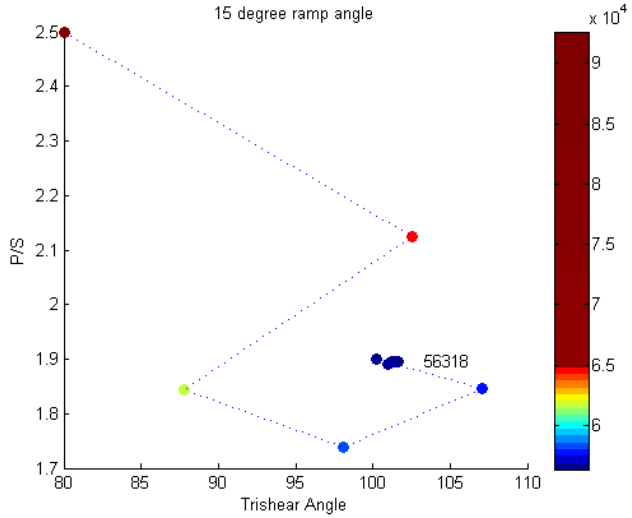

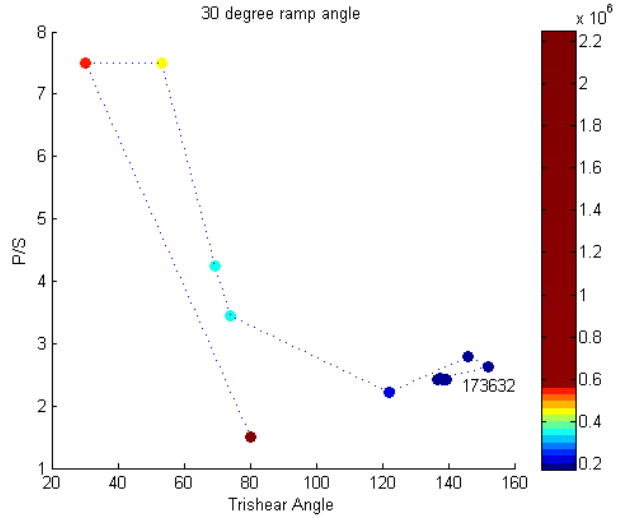

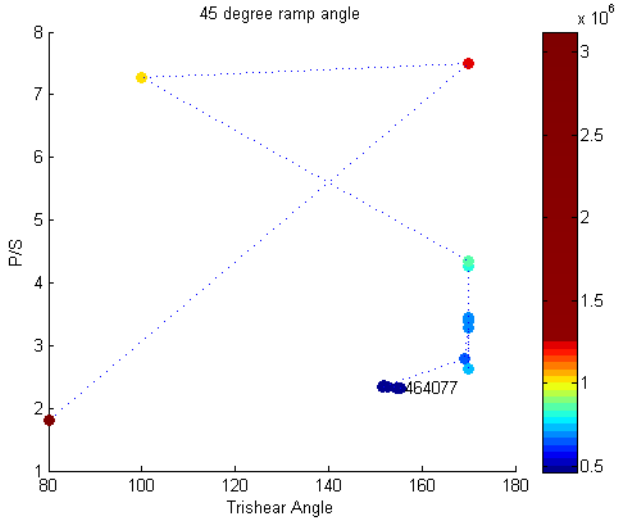

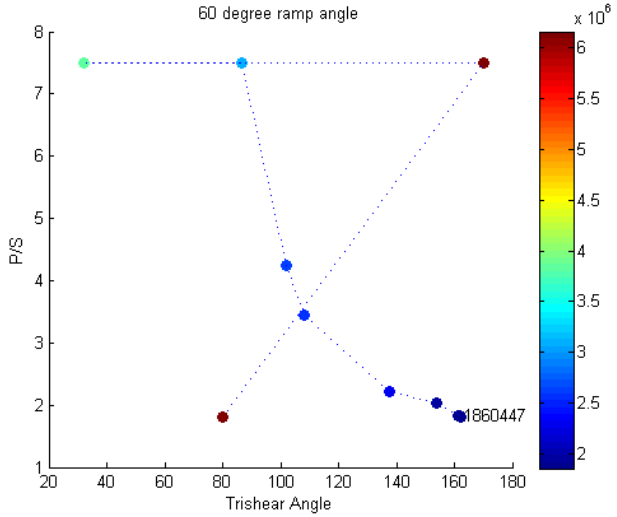

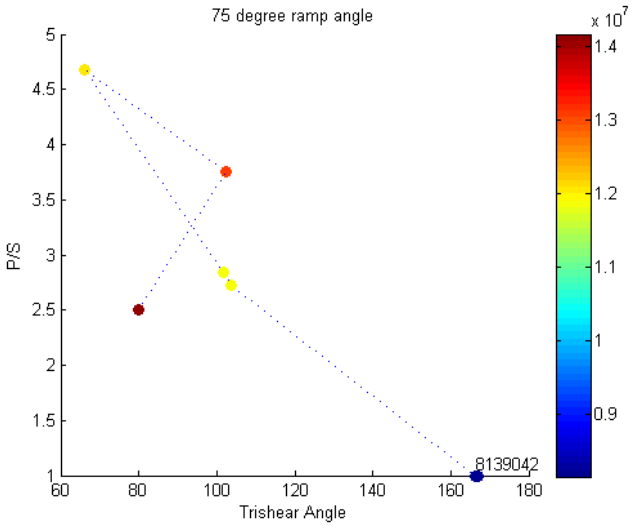

Figure 7: Plots of trishear angle and propagation-to-slip ratio parameter space for five trishear inverse models. The color of each point refers to the value of χ^2 at each iteration with the dotted line showing the path from each iteration to the next. Refer to Table 2 for specific parameter values. The P/S parameter was allowed to vary between 1.0 and 7.5. The trishear angle could vary between 30° and 170°.

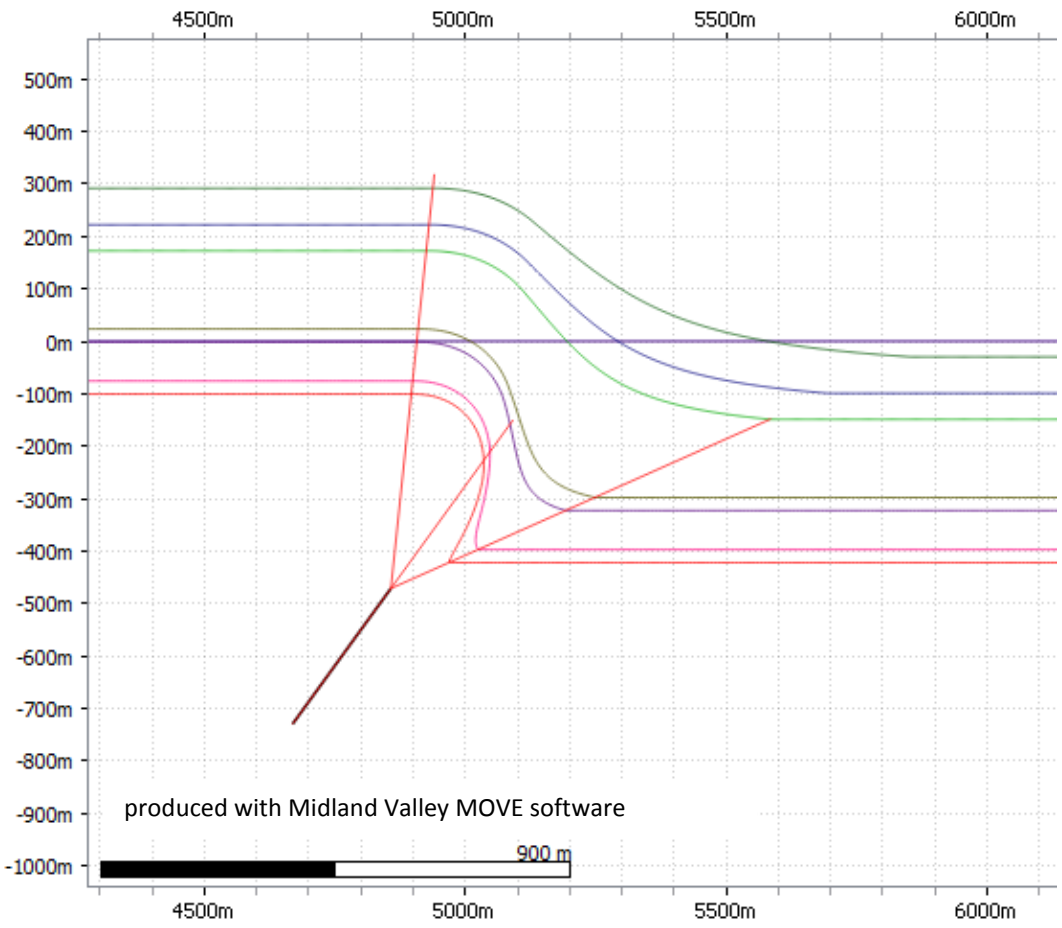

Figure 8. Simple model of trishear, using fictional horizons. The longer red lines represent the boundaries of the trishear zone with the bisecting line representing the path of fault propagation. Note the lack of a backlimb fold without a flat-to-ramp transition in the fault surface at depth.

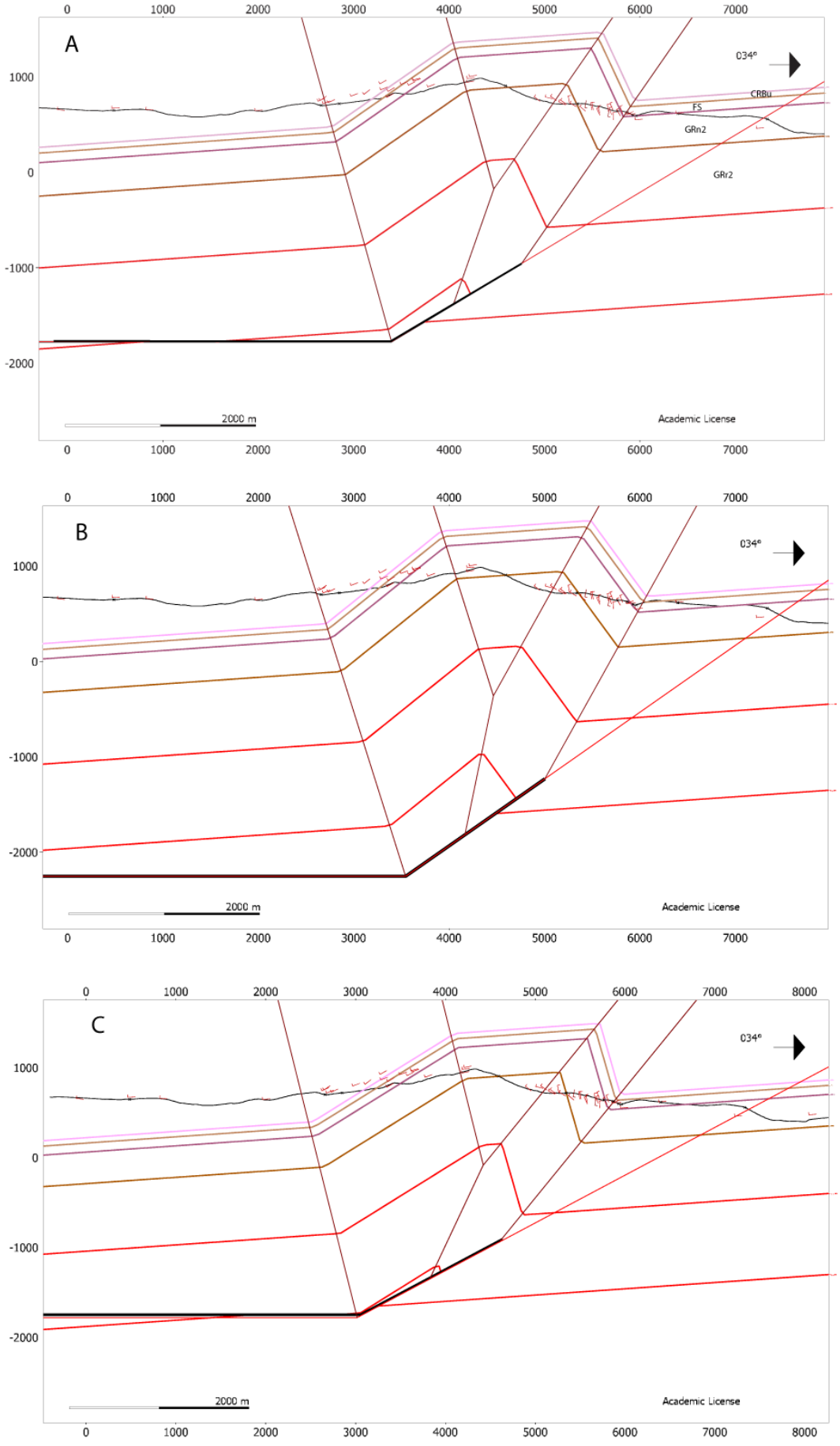

Figure 9:
Cross sections through Umtanum Ridge west of Yakima Canyon (see map for location). (A), (B), and (C) show mean, maximum, and minimum values, respectively, for the interlimb angle (γ) in the case where the master fault has not propagated to the surface. See text for discussion.
Figures contain same stratigraphy as map with the top and bottom of the lower CRBG units (pre GRr2) shown in red. Dip-tics (red) and contacts (black crosses) have been projected onto section based on map. Vertical units are meters above sea level. Horizontal units are meters northeast of cross section origin.
Figures produced using Midland Valley's Move software.

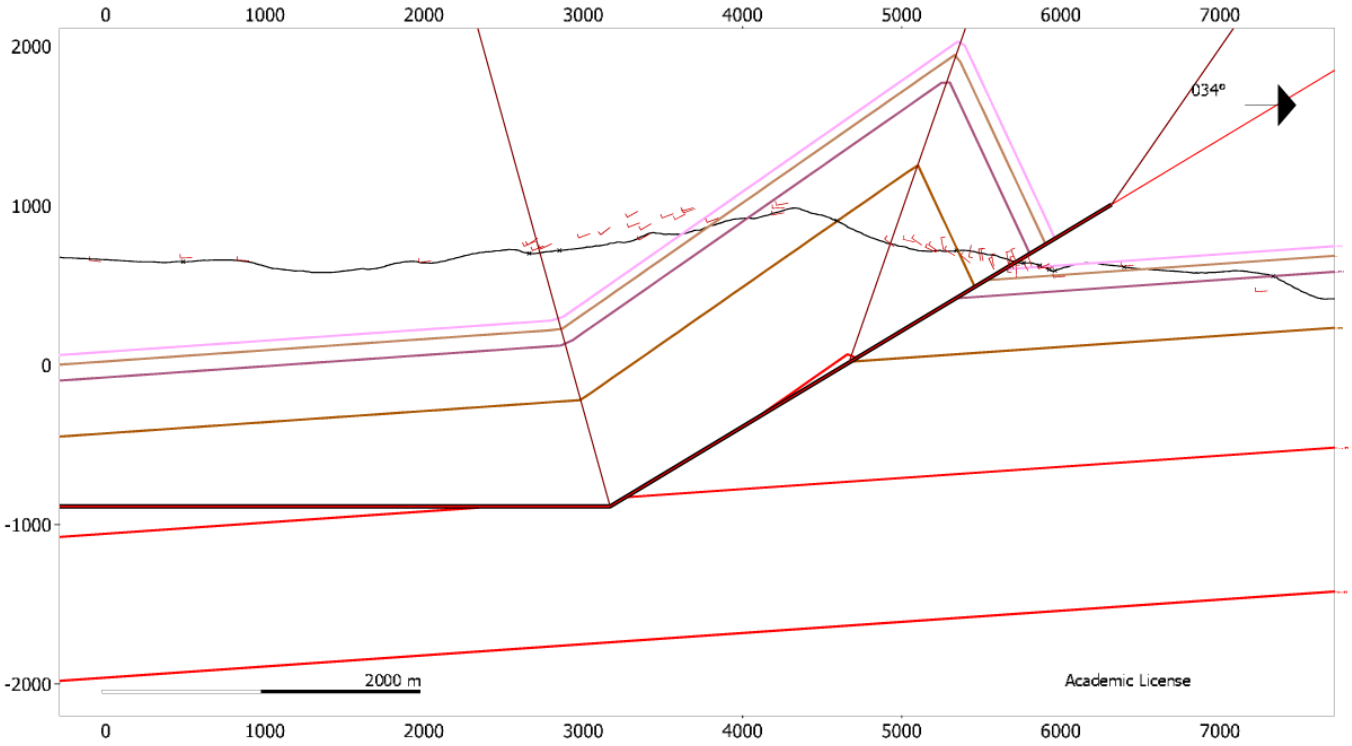

Figure 10. Same line of section from Figure 9, but for the case where the master fault has propagated to the surface. See text for discussion.

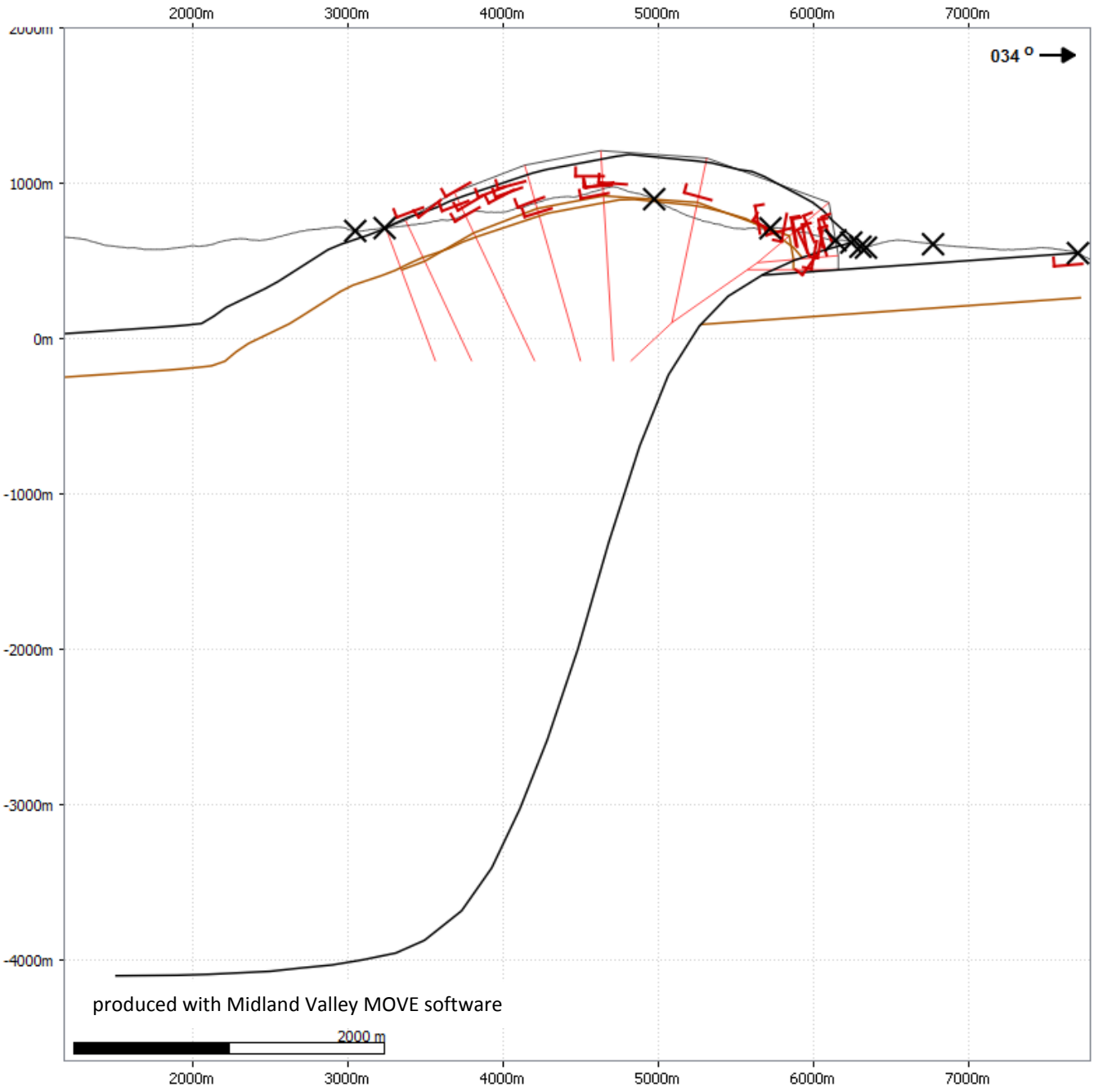

Figure 11: Cross section through Umtanum Ridge showing the fault geometry which best reproduces the observed shape of unit GRn2 (black line) with 460 m of displacement, producing the fault-bend fold seen here. See Figure 4 for a more detailed view of the observed geometry and for symbol explanation.

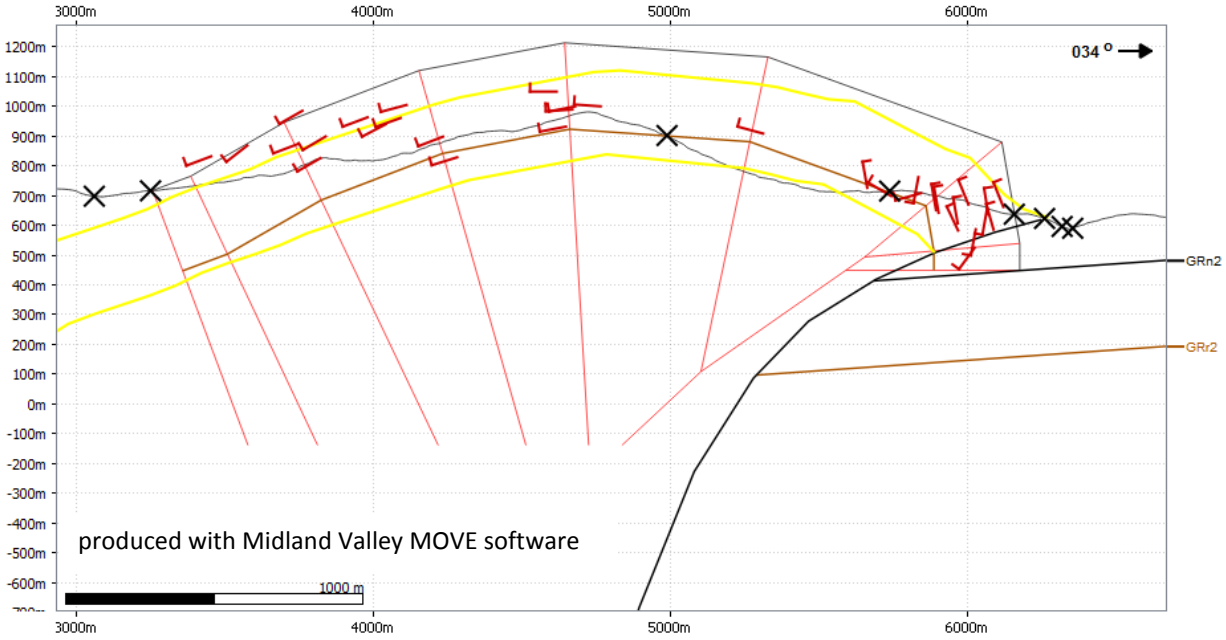

A

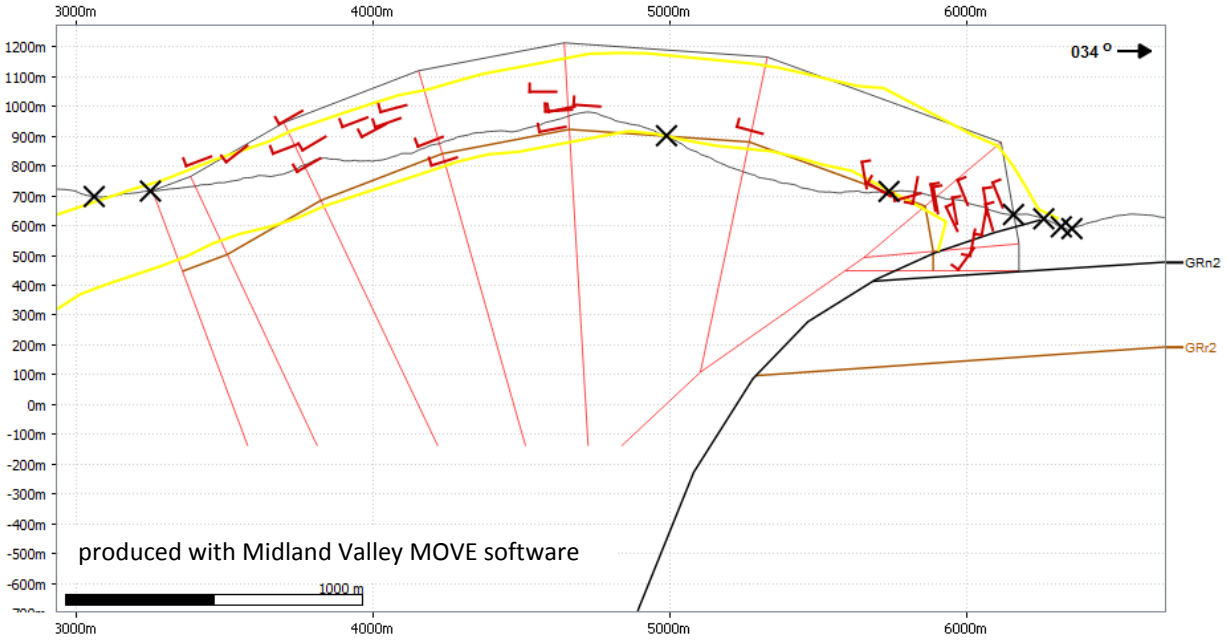

B

Figure 12: The hybrid model. Modeled horizons are highlighted in yellow. Observed horizons are brown and black. (A) Fold formation begins with 410 m of fault-bend fold displacement along fault, producing southern limb and gently dipping north limb. Followed by 110 m of trishear slip (B), producing overturning of at least the lower horizon. If the fault propagated above the current topographic surface, overturning of the upper horizon could occur.

Bedrock Geologic Map of the Yakima River Canyon, Kittitas and Yakima Counties, Washington

By
Brendan A Miller

Legend

Unit Contact

- Map boundary
- Line of section
- Contact--identity or existence questionable, location inferred
- Contact--identity or existence questionable, location approximate
- Contact--identity or existence questionable, location accurate
- Contact--identity and existence certain, location inferred
- Contact--identity and existence certain, location approximate
- Contact--identiy and existence certain, location accurate
- Thrust fault--identity and existance certain, location approximate
- Thrust fault--identity and existence certain, location concealed

upright attitude

- field measured, horizonal
- lidar measured
- field measured

overturned attitude

- lidar measured
- field measured

Unit

- Qu--Quaternary undifferentiated
- CRBu--Upper flows of Columbia River Basalt Group (see text)
- FS--Frenchman Springs Member, Wanapum Basalt
- GRn2--Upper flows of normal polarity, Grande Ronde Basalt
- GRr2--Upper flows of reversed polarity, Grande Ronde Basalt